**THE EUROPEAN
PHYSICAL JOURNAL D**

Regular Article

Hydrogenated gold clusters from helium nanodroplets: displacement of H_2 by $H_2O^\star$

Linnea Lundberg[1], Paul Martini[1], Marcelo Goulart[1], Michael Gatchell[1,2], Diethard K. Bohme[3], and Paul Scheier[1,a]

[1] Institut für Ionenphysik und Angewandte Physik, Universität Innsbruck, Technikerstr. 25, 6020 Innsbruck, Austria
[2] Department of Physics, Stockholm University, 106 91 Stockholm, Sweden
[3] Department of Chemistry, York University, Toronto, ON M3J 1P3, Canada

Abstract. Cationic clusters of gold, containing up to 8 atoms, and decorated with molecular hydrogen and water, were investigated with mass spectrometry. The clusters were grown as neutrals in superfluid helium nanodroplets that were ionized by electron impact. The resulting gas phase cluster cations exhibit magic sizes corresponding to the number of H_2 molecules that form the first solvation layer, consistent with previous findings. The presence of water is found to efficiently displace hydrogen, one H_2 molecule for each H_2O. Our calculations show that the binding energy of water to the charged gold clusters is about twice as large as for hydrogen, though this depends on the charge of the clusters. This suggests that residual water could reduce the efficiency for metal particles to chemically store hydrogen gas, a promising technique for hydrogen fuel storage.

1 Introduction

The use of metal nanoparticles for high density H_2 storage is becoming increasingly relevant in modern fuel technology. Storing hydrogen gas in quantities required for, e.g. fuel cells, traditionally requires storing large amounts of the flammable gas in high pressure vessels, which involves undesired risks in commercial applications. An alternative approach involves chemical storage of hydrogen in a reversible fashion, so that the bound H_2 molecules can be released back into the gas phase before being extracted for use [1]. Particles of transition metals and their alloys are promising in this regard because of their moderate bond strengths with H_2 [2], which allows the bonds to be formed and broken by small changes in temperature and pressure [1,3]. A disadvantage of purely metallic matrices for hydrogen storage is the weight and cost of the (often precious) metals used [1], but this can be, at least partially, overcome by doping other materials with metal nanoparticles. Examples of this include the doping of carbon matrices with metal particles, as small as one or a few atoms, that act as nucleation sites for binding H_2 [4–6]. In this light, nanosize effects have become an important research focus as has nanoparticle protection against oxidation by O_2 and H_2O, for example by using semipermeable pro-

tective layers that still allow H_2 to easily penetrate [1,7]. While platinum group metals have received much attention in hydrogen storage applications [1,5,6], gold too has become of interest as a substrate for H_2 storage because of its catalytic activity [8].

Previous experiments in our laboratory [9] have shown that H_2 molecules readily attach to gold clusters with up to at least 8 gold atoms when captured by superfluid helium nanodroplets. Helium nanodroplets are miniature cryo-vessels with equilibrium temperatures of 0.37 K that are extremely versatile for growing cold clusters from atomic and molecular building blocks [10,11]. Their high thermal conductivity and low temperatures mean that any captured dopants will be efficiently cooled to the temperature of the liquid and readily condense into clusters [10,11]. Using this technique to form hydrogenated gold clusters, the clusters were readily ionized by the presence of electron acceptors such as He^+ or proton donors such as HeH^+ following electron impact on the doped droplets, after which some H_2 elimination ensued due to the high excess energy of these processes [9]. There was no evidence for the dissociation of adsorbed H_2 molecules in that there was no indication of H elimination that might result from dissociation. The hydrogenated gold cluster ion distributions exhibited "magic" features that appear to reflect special stabilities for certain numbers of adsorbed H_2 molecules depending on the structure of the underlying (most often computed to be flat) Au cluster skeleton and the number of Au atoms exposed on the periphery. Shifts in magic numbers were suggested to reflect transitions

from 2D to 3D structures as the cluster size increases. The computed H_2 affinities of the cationic clusters were as high as $1.1\,eV$, but weakened with increasing cluster size [9].

Interestingly, we noted in these experiments that some residual water molecules became embedded in the hydrogenated gold clusters, apparently displacing more weakly bound hydrogen molecules. This led to an observed shift in the "magic" numbers corresponding to the reduction of the number of adsorbed hydrogen molecules by one for each additional water molecule. These observations provided an opportunity to investigate the "poisoning" of H_2 storage by water molecules and this is the focus of the experimental and theoretical study reported here.

2 Methods

2.1 Experimental details

An overview of the procedures involved in our experiments is provided schematically in Figure 1. A continuous beam of neutral He droplets was formed by the expansion of pre-cooled He gas (Messer, 99.9999% purity) with a backing pressure of 22.5 bar into vacuum through a nozzle with an inner diameter of $5\,\mu m$ that was cooled to $9.55\,K$ by a two stage, closed circuit helium cryocooler (SRDK-415D-F50H, Sumitomo Heavy Industries Ltd.). Under these conditions, droplets were formed following a broad log-normal size distribution and with a mean size on the order of 10^6 He atoms. The central part of the beam then passed through a 0.8 mm diameter skimmer located 8 mm downstream from the nozzle before traversing a pair of sequentially pumped pickup chambers. In the first pickup chamber, molecular hydrogen gas (Messer Austria GmbH, purity 99.999%) was introduced by a gas line controlled with a needle valve. H_2 molecules along the flight path of the He droplet beam were captured by the droplets where they were cooled to the $0.37\,K$ equilibrium temperature of the liquid and could condense into clusters. Residual water molecules in the hydrogen gas line and from the walls of the pickup chamber were incorporated in the droplets too. The second pickup chamber, located 115 mm after the first one, housed an oven with a heating power of 118 W for evaporating solid gold at a temperature of approximately $950°C$. The design of this oven is similar to the one reported by Feng et al. [12]. The gold vapor, mostly consisting of individual Au atoms, was picked up by the He droplets to condense together with the H_2/H_2O mixture already present therein. The vapor pressures in the two pickup cells were both on the order of 10^{-6} mbar.

The doped droplets were ionized by the impact of 85 eV electrons in a Nier-type ion source. When the droplets are struck by an electron, He^+ is the main initial product. This charge then migrates through the droplet via resonant hole-hopping, on average about 10 times, until a He_2^+ is expected to be formed (unless a dopant is encountered first) [13]. This ion may then be attracted by the dopants, which have higher polarizabilities than the surrounding He. Since the ionization energy of He is much higher than
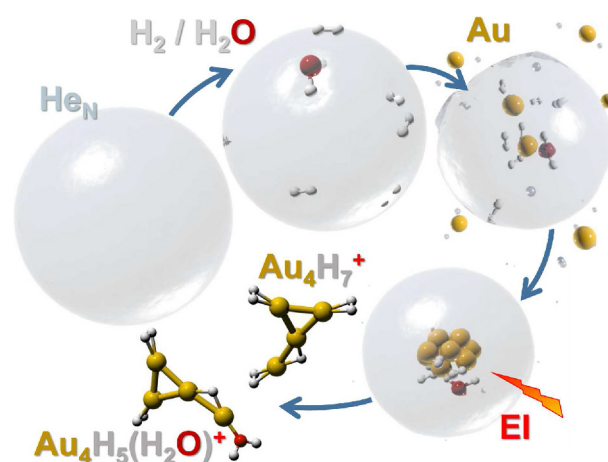

Fig. 1. Schematic overview of the steps involved in our experimental procedure. Starting from the top left and continuing clockwise, neutral droplets containing millions of He atoms interact with and capture gas phase water and hydrogen molecules and then gold atoms. The droplets are ionized by electron impact (EI) which produces cationic dopants that are subsequently ejected from the droplets. These are then detected with a time-of-flight mass spectrometer.

most dopants, the interaction between the He_2^+ (or He^+) ion and the dopant will lead to a highly exothermic charge transfer reaction. The excess energy will heat the dopant cluster and have a strong influence on their final structures as they then cool. The measurable properties of the final products thus represent primarily their cationic forms, e.g. with regard to magic numbers, with the precise structures of their neutral precursors being of lesser importance. This method of ionizing He droplets typically deposits several charges to the droplets [14]. Charges in excess of the stability limit of the droplets will be expelled into the gas phase as the multiply charged droplets stabilize [14]. It is these gas phase charge carriers that we detect in our measurements.

Positively charged products were analyzed using a reflectron time-of-flight mass spectrometer (Tofwerk AG, model HTOF) with a rated resolution of $m/\Delta m = 5000$. The recorded mass spectra were evaluated using the IsotopeFit software [15]. IsotopeFit is a tool for analyzing mass spectra that corrects for isotopic distributions and can deconvolute overlapping cluster distributions, allowing the user to extract the corrected abundances of different species. Additional experimental details can be found in references [16–18].

2.2 Theoretical details

Cluster geometries were determined using electronic structure calculations with the Gaussian 16 software package [19]. Second order Møller-Plesset (MP2) perturbation theory was used together with a def2-TZVP triple zeta basis set. For the Au atoms, core potentials belonging to this basis set were used for the inner electron shells that contain corrections for relativistic effects and speed up the
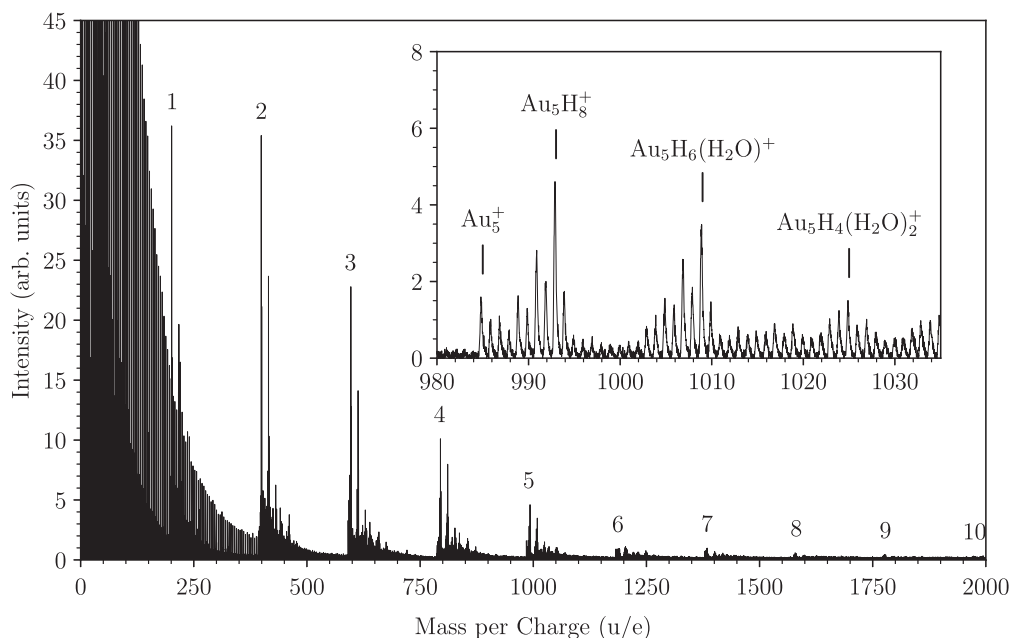
Fig. 2. Mass spectrum of cationic clusters formed from helium nanodroplets doped with H_2, atomic Au, and residual H_2O molecules and ionized by electron impact at $85\,\mathrm{eV}$. The start of each cluster group is labeled by the number of gold atoms they contain. The dominating species are $Au_nH_x^+$ clusters. At masses up to about $500\,\mathrm{u}$, the tail of the He_n^+ cluster series is clearly visible. The inset is a close-up in which the water content of the clusters is easily seen.

calculations. The optimized structures were also evaluated with a vibrational analysis to determine that real potential energy minima were obtained and to determine the zero-point energy corrections. The initial structures of the studied clusters were based on geometries determined for pure gold clusters and complexes of gold and hydrogen, previously calculated at the same level of theory, which were re-optimized following the addition of water molecules [9]. Other tested structures did not result in more energetically favorable structures.

3 Results and discussion

Figure 2 shows the intensity distribution obtained mass-spectrometrically for hydrogenated gold cluster cations with trace amounts of residual water content. The dominant species in the mass spectrum are He_n^+ clusters, fragments of the large droplets from which the clusters are formed, and the series of hydrogenated gold clusters. However, substantial peaks are also observed for $Au_nH_x(H_2O)_y^+$ ions (with $y = 1$ and 2) among the many peaks for $Au_nH_x^+$ ions. An example of this is shown (for $n = 5$) in the inset of Figure 2. We do see some evidence of 3 water molecules binding to the $Au_nH_x^+$ clusters as well, but the weak signal and overlap with systems containing fewer water molecules and more hydrogen (with the same mass) make it difficult to reliably determine their abundances.

The panels in Figure 3 present measured size distributions extracted from the mass spectrum in Figure 2. Three series are shown for each gold cluster size from $n = 1$–8: purely hydrogenated $Au_nH_x^+$ clusters for x from 1 up to

20 (from Ref. [9]), and hydrogenated cationic gold clusters containing one and two water molecules, $Au_nH_x(H_2O)^+$ and $Au_nH_x(H_2O)_2^+$, respectively. The presence of oscillations and intense "magic" numbers in the distributions of the $Au_nH_x^+$ cluster sizes have been discussed previously [9]. The deviating trend in magic numbers with respect to hydrogenation for clusters containing 7 or more Au atoms were in the previous study suggested to reflect transitions from 2D to 3D structures as the cluster size increases. The addition of water molecules to the clusters shift the magic numbers of H atoms by 2 for each molecule that is added, at least for clusters sizes of $n < 7$. For $n = 7$ and 8, the trend is less clear but suggests that the effect of adding water to the clusters is weakened, although the increasing statistical uncertainties make it prohibitive to draw any strong conclusions.

For cluster sizes up to $n = 6$, the shift in the magic number of H atoms by two indicates that the water is effectively replacing one H_2 molecule. The process appears to be rather strong since the amount of water present in the experiment is expected to be considerably lower than the amount of hydrogen. Despite this, the yield of clusters containing a single water is of the same order of magnitude as the purely hydrogenated gold clusters. Another feature of the water-containing clusters is the enhancement of sizes larger than the magic numbers. This is most clear for larger systems (higher n) in which a second maximum is present in the range of $10 \leq x \leq 15$. The magic numbers shown in Figure 3 signify the saturation of the gold clusters with hydrogen, effectively closing the first and most tightly bound solvation layer [9]. The second hump could be indicative of a second solvation layer, but
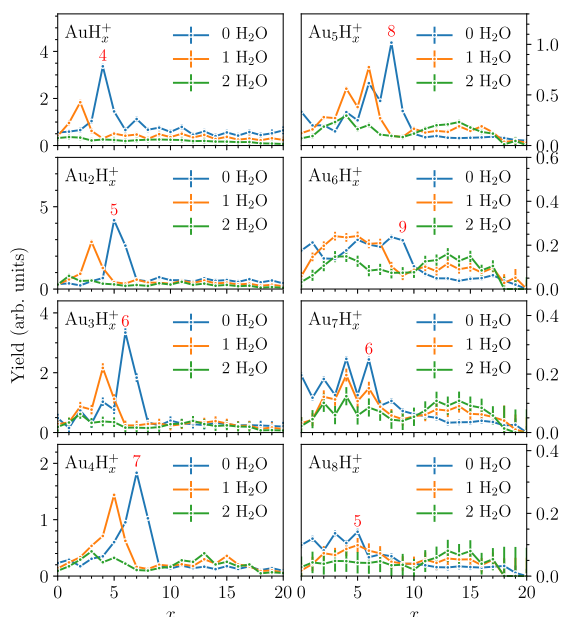
Fig. 3. Extracted size distributions for cationic gold clusters complexed with H_2 and H_2O. The blue series are for systems with no water (from Ref. [9]), the orange series are for clusters containing a single water molecule and x hydrogen atoms, while the green series (not present in all panels) are for cluster containing two water molecules. Magic sizes corresponding to the saturation of Au–H bonds are labelled with red numbers indicating the number of H atoms for each gold cluster size.

the role of water is not clear from the experimental data. One possibility is that the permanent dipole moment of the H_2O molecules allows for a stronger interaction of the outer solvation layers with the ionic cores of the clusters compared to the non-polar H_2. This would presumably only play a role if water molecules were present in the outer solvation layer.

3.1 Computed structures of hydrogenated and hydrated gold cluster cations

Figures 4 and 5 display the calculated structures for some of the most abundant "magic" clusters of $Au_nH_x^+$ with $n = 1$–3 and $n = 4$–6, respectively, in which up to 3 H_2 molecules are sequentially displaced by H_2O. All the structures that are shown are planar in regard to the positions of the Au atoms. The calculations suggest that H_2O molecules, like H_2, bind directly to Au atoms of the gold cluster "skeleton" and that the extra H atom in the even-numbered gold clusters ($n = 2$, 4, and 6) simply bridges two Au atoms, giving a closed shell electronic structure. The geometries of the protonated, even-numbered clusters show a strong resemblance to the next larger gold cluster size (except for differences in the Au–H vs. Au–Au bond distances). This is consistent with the similarities seen in Au and H chemistry, where gold atoms often behave as "large" hydrogen atoms [20–25]. The structures in which H_2O molecules have displaced H_2 units show essentially no change in their overall geometries; the water is effectively a
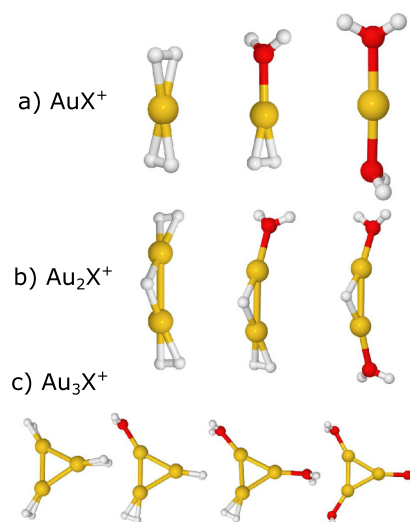

Fig. 4. Proposed structures for a selection of gold-hydrogen-water clusters from MP2/def2-tzvp level calculations. Starting from the optimized pure gold-hydrogen clusters [9], one, two or three H_2 molecules have been replaced by H_2O before the structures were re-optimized. The following structures are shown: (a) AuH_4^+, $AuH_2(H_2O)^+$, $Au(H_2O)_2^+$; (b) $Au_2H_5^+$, $Au_2H_3(H_2O)^+$, $Au_2H(H_2O)_2^+$; c) $Au_3H_6^+$, $Au_3H_4(H_2O)^+$, $Au_3H_2(H_2O)_2^+$, $Au_3(H_2O)_3^+$.
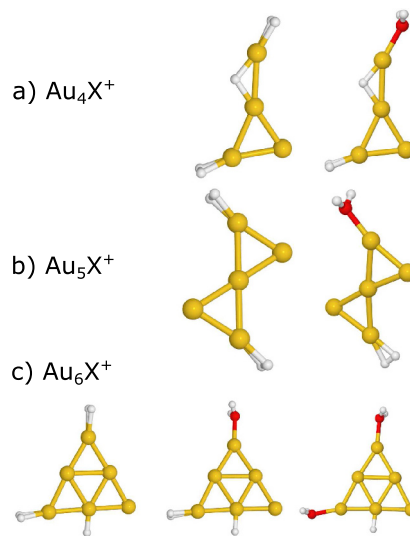

Fig. 5. Proposed structures for a selection of gold-hydrogen-water clusters from MP2/def2-tzvp level calculations. Starting from the optimized pure gold-hydrogen clusters [9], one, two or three H_2 molecules have been replaced by H_2O before the structures were re-optimized. The following structures are shown: (a) $Au_4H_5^+$, $Au_4H_3(H_2O)^+$; (b) $Au_5H_4^+$, $Au_2H_2(H_2O)^+$; (c) $Au_6H_5^+$, $Au_6H_3(H_2O)^+$, $Au_6H(H_2O)_2^+$. In the cases where different H_2 molecules could be substituted, the one which gave the lowest total energy is shown.

1:1 replacement for the hydrogen. From a structural standpoint this explains the shift by 2H atoms seen in the cluster yields in Figure 3 for each additional water molecule. In the limit of fully hydrated clusters, these results are in good agreement with previous results [26,27].
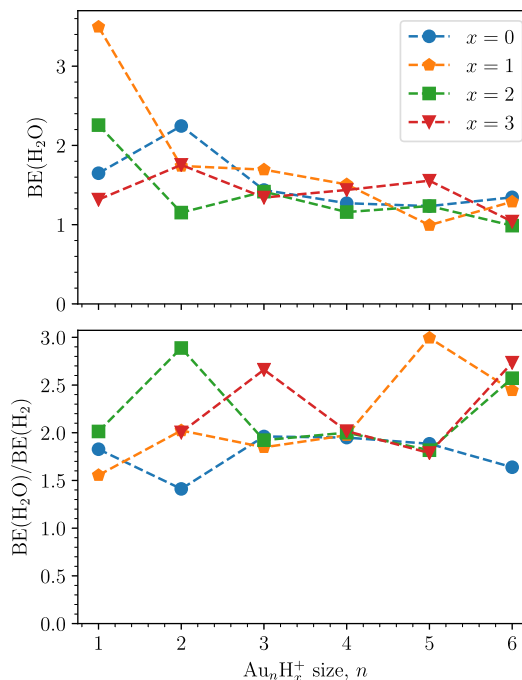
Table 1. The binding energy of an H_2O molecule bound to different sized gold-hydrogen clusters. The values in parenthesis are the ratios between the binding energy of H_2O and that of H_2: $BE(H_2O)/BE(H_2)$.

B.E. of H_2O to:	$X = -$	$X = H$	$X = H_2$	$X = H_3$
AuX^+	1.65 eV (1.83)	3.50 eV (1.56)	2.26 eV (2.01)	–
Au_2X^+	2.25 eV (1.41)	1.74 eV (2.02)	1.15 eV (2.89)	1.75 eV (2.00)
Au_3X^+	1.44 eV (1.96)	1.69 eV (1.85)	1.42 eV (1.92)	1.34 eV (2.66)
Au_4X^+	1.27 eV (1.95)	1.51 eV(1.97)	1.16 eV (2.00)	1.44 eV (2.02)
Au_5X^+	1.23 eV (1.88)	0.99 eV (2.99)	1.24 eV (1.82)	1.55 eV (1.79)
Au_6X^+	1.35 eV (1.64)	1.29 eV (2.44)	0.99 eV (2.57)	1.04 eV (2.73)

Table 1 summarizes our computed values for the H_2O affinity for small Au clusters that are hydrogenated to varying degrees, $Au_nH_x(H_2O)^+$. We show graphically in the top panel of Figure 6 the variation of the H_2O affinity, $BE(H_2O)$, the values displayed in Table 1. In the lower panel of Figure 6 we also show the calculated magnitude of the H_2O affinity relative to the H_2 affinity, $BE(H_2O)/BE(H_2)$, for different extents of hydrogenation. Much like the binding energies of hydrogen atoms and molecules to gold clusters [9], the binding energy of water is highest for small gold clusters. For a single Au^+ the binding energies range between 1.32 eV and 3.50 eV depending on the degree of hydrogenation. The spread in binding energies decreases with increasing cluster size. For the largest clusters calculated in this study, containing 6 Au atoms, the energies range between from 0.99 eV for $Au_6H_2^+$ and 1.35 eV for Au_6^+ when interacting with a single H_2O molecule.

As has been seen for other cationic gold-ligand complexes [28], our calculations indicate that the gold clusters preferentially form bonds with the one of the lone electron pairs on the O atom of the water molecules. For the structures studied here, the binding energy of the water molecule is on average 2.1 ± 0.4 times higher than the equivalent binding energy of an additional hydrogen molecule (see Tab. 1 and the lower panel of Fig. 6). Among these values there are some individual outliers, e.g., $Au_2H_2^+$ and A_5H^+ where the binding energy of H_2O is close to three times higher than for H_2. Similarly, the ratio for Au_2^+ is only 1.4. These deviations appear mostly for open shell systems, which in general have weaker binding energies and larger relative fluctuations in the interaction energies between complex sizes. The structures of the Au skeletons are also more readily distorted by the attachment of ligands for the open shell systems. A similar effect was also seen for Au clusters interacting with imidazole [28] molecules, where open shell systems often had the loss of Au atoms as their lowest dissociation pathway instead the loss of ligand molecules. For the closed shell systems (i.e. odd numbers of Au atoms matched with even numbers of H atoms and vice versa), we instead see more consistent binding energies of both H_2O and H_2 adducts for all cluster sizes.

For comparison, we have also performed test calculations (for a few select geometries, not an exhaustive survey) of neutral gold dimers and trimers interacting with H_2 or H_2O. These showed that the binding energies are significantly lower than for the charged clusters, between 0.5 eV and 0.8 eV depending on the structure. As for the

Fig. 6. Top panel: calculated binding energies of a H_2O molecule to $Au_nH_x^+$ for different values of n and x. Lower panel: the binding energies of an H_2O molecule compared to the binding energies of an H_2 molecule, $BE(H_2O)/BE(H_2)$, for the same parent clusters as in the upper panel.

charged clusters, the water forms a stronger bond with the gold cluster than the hydrogen, but the ratio of binding energies is lower, with the highest being 1.3 for the neutral gold dimer. The relative interaction energies of water and hydrogen are thus dependent on the partial charges of the gold atoms in the cluster, which could potentially be tuned for metal particles in matrices.

4 Conclusions

Previously we demonstrated experimentally that H_2 molecules readily attach to cationic gold clusters with up to at least 8 gold atoms that are formed from neutral parents grown in a He environment near zero K. Here we see that trace amounts of ambient water molecules can displace the adsorbed H_2. The computed H_2 affinities of the cation clusters are as high as 1.1 eV, but the equivalent

H_2O affinities are here shown to be on average about two times higher for all cluster sizes. Despite the higher interaction energies, the water molecules do not significantly alter the structures of the hydrogenated gold clusters. In both cases, all of the lowest energy structures containing up to at least 6 gold atoms are found to be planar (with regard to the gold "skeleton"). In the experiments, the displacement of hydrogen molecules by water is evident from the shift in magic numbers associated with the closure of the first solvation shell by 2H atoms for each additional water molecule. This is true for cluster size up to 6 Au atoms, after which the trend is less clear. This switch occurs at the same size as the previously reported [9,29] transition from 2D structures of the Au "skeletons" to 3D geometries with increasing cluster size. These findings are also consistent with previous studies on gold-water complexes [26,27].

Our findings show that even trace amounts of water can interfere with the binding of molecular hydrogen to metal nanoparticles, and that this effect is charge dependent. For applications in hydrogen storage, our results indicate that nucleation sites used for binding H_2 could be susceptible to "poisoning" by much more tightly bound H_2O molecules, limiting the amount of hydrogen that can be stored in the presence of water. Technologies are available to alleviate this potential problem [7]. However, this also opens the potential for applications in which the displacement of hydrogen by water is exploited. For example, water could be used to extract hydrogen stored on metal nanoparticles, where H_2O spontaneously triggers the release of H_2 from the surface. This process could then later be reversed by baking the system to evacuate the water before replenishing the storage device with hydrogen.

Author contribution statement

The measurements were performed by P. Martini and M. Goulart. The calculations were performed by L. Lundberg. The data were evaluated and visualized by L. Lundberg and M. Gatchell. The manuscript was written and reviewed by M. Gatchell, D. K. Bohme, and P. Scheier. All the authors have read and approved the final manuscript.

References

1. M. Yamauchi, H. Kobayashi, H. Kitagawa, ChemPhysChem **10**, 2566 (2009)
2. C.D. Gelatt, H. Ehrenreich, J.A. Weiss, Phys. Rev. B **17**, 1940 (1978)
3. M.S. Dresselhaus, I.L. Thomas, Nature **414**, 332 (2001)
4. T. Hussain, B. Pathak, M. Ramzan, T.A. Maark, R. Ahuja, Appl. Phys. Lett. **100**, 183902 (2012)
5. Y. Li, R.T. Yang, J. Phys. Chem. C **111**, 11086 (2007)
6. C.M. Ramos-Castillo, J.U. Reveles, R.R. Zope, R. de Coss, J. Phys. Chem. C **119**, 8402 (2015)
7. E.S. Cho, A.M. Ruminski, S. Aloni, Y.S. Liu, J. Guo, J.J. Urban, Nat. Commun. **7**, 10804 (2016)
8. C.T. Campbell, Science **306**, 234 (2004)
9. L. Lundberg, P. Martini, M. Goulart, M. Gatchell, D.K. Bohme, P. Scheier, J. Am. Soc. Mass Spectrom. **30**, 1906 (2019)
10. A. Mauracher, O. Echt, A.M. Ellis, S. Yang, D.K. Bohme, J. Postler, A. Kaiser, S. Denifl, P. Scheier, Phys. Rep. **751**, 1 (2018)
11. J.P. Toennies, A.F. Vilesov, Angew. Chem. Int. Ed. **43**, 2622 (2004)
12. C. Feng, E. Latimer, D. Spence, A.M.A.A. Al Hindawi, S. Bullen, A. Boatwright, A.M. Ellis, S. Yang, Phys. Chem. Chem. Phys. **17**, 16699 (2015)
13. A.M. Ellis, S. Yang, Phys. Rev. A **76**, 032714 (2007)
14. F. Laimer, L. Kranabetter, L. Tiefenthaler, S. Albertini, F. Zappa, A.M. Ellis, M. Gatchell, P. Scheier, Phys. Rev. Lett. **123**, 165301 (2019)
15. S. Ralser, J. Postler, M. Harnisch, A.M. Ellis, P. Scheier, Int. J. Mass Spectrom. **379**, 194 (2015)
16. H. Schöbel, P. Bartl, C. Leidlmair, S. Denifl, O. Echt, T.D. Märk, P. Scheier, Eur. Phys. J. D **63**, 209 (2011)
17. T. Kurzthaler, B. Rasul, M. Kuhn, A. Lindinger, P. Scheier, A.M. Ellis, J. Chem. Phys. **145**, 064305 (2016)
18. M. Kuhn, M. Renzler, J. Postler, S. Ralser, S. Spieler, M. Simpson, H. Linnartz, A.G.G.M. Tielens, J. Cami, A. Mauracher, et al., Nat. Commun. **7**, 13550 (2016)
19. M.J. Frisch, G.W. Trucks, H.B. Schlegel, G.E. Scuseria, M.A. Robb, J.R. Cheeseman, G. Scalmani, V. Barone, G.A. Petersson, H. Nakatsuji, et al., *Gaussian 16 Rev. a.03* (2016)
20. E. Zeller, H. Beruda, A. Kolb, P. Bissinger, J. Riede, H. Schmidbaur, Nature **352**, 141 (1991)
21. H. Schmidbaur, O. Steigelmann, Z. Naturforsch. B **47**, 1721 (1992)
22. K. Angermaier, H. Schmidbaur, Inorg. Chem. **33**, 2069 (1994)
23. H. Schmidbaur, S. Hofreiter, M. Paul, Nature **377**, 503 (1995)
24. D. Benitez, N.D. Shapiro, E. Tkatchouk, Y. Wang, W.A. Goddard III, F.D. Toste, Nat. Chem. **1**, 482 (2009)
25. L.S. Wang, Phys. Chem. Chem. Phys. **12**, 8694 (2010)
26. J.U. Reveles, P. Calaminici, M.R. Beltrán, A.M. Köster, S.N. Khanna, J. Am. Chem. Soc. **129**, 15565 (2007)
27. T. Nagata, F. Mafuné, J. Phys. Chem. C **121**, 16291 (2017)
28. M. Gatchell, M. Goulart, L. Kranabetter, M. Kuhn, P. Martini, B. Rasul, P. Scheier, Phys. Chem. Chem. Phys. **20**, 7739 (2018)
29. D. Schooss, P. Weis, O. Hampe, M.M. Kappes, Philos. Trans. R. Soc. London A: Math. Phys. Eng. Sci. **368**, 1211 (2010)